

# Doping influence of spin dynamics and magnetoelectric effect in hexagonal $Y_{0.7}Lu_{0.3}MnO_3$

W. Tian,<sup>1,\*</sup> Guotai Tan,<sup>2,†</sup> Liu Liu,<sup>2</sup> Jinxing Zhang,<sup>2</sup> Barry Winn,<sup>1</sup> Tao Hong,<sup>1</sup> J. A. Fernandez-Baca,<sup>1,3</sup> Chenglin Zhang,<sup>3,4</sup> and Pengcheng Dai<sup>3,4</sup>

<sup>1</sup>Quantum Condensed Matter Division, Oak Ridge National Laboratory, Oak Ridge, Tennessee 37831, USA

<sup>2</sup>Department of Physics, Beijing Normal University, Beijing 100875, China

<sup>3</sup>Department of Physics and Astronomy, The University of Tennessee, Knoxville, Tennessee 37996, USA

<sup>4</sup>Department of Physics and Astronomy, Rice University, Houston, Texas 77005, USA

(Dated: June 13, 2021)

We use inelastic neutron scattering to study spin waves and their correlation with the magnetoelectric effect in  $Y_{0.7}Lu_{0.3}MnO_3$ . In the undoped  $YMnO_3$  and  $LuMnO_3$ , the Mn trimerization distortion has been suggested to play a key role in determining the magnetic structure and the magnetoelectric effect. In  $Y_{0.7}Lu_{0.3}MnO_3$ , we find a much smaller in-plane (hexagonal  $ab$ -plane) single ion anisotropy gap that coincides with a weaker in-plane dielectric anomaly at  $T_N$ . Since both the smaller in-plane anisotropy gap and the weaker in-plane dielectric anomaly are coupled to a weaker Mn trimerization distortion in  $Y_{0.7}Lu_{0.3}MnO_3$  comparing to  $YMnO_3$  and  $LuMnO_3$ , we conclude that the Mn trimerization is responsible for the magnetoelectric effect and multiferroic phenomenon in  $Y_{1-y}Lu_yMnO_3$ .

PACS numbers: 75.30.Ds, 75.40.Gb, 75.50.Ee, 75.85.+t

Driven by modern technology towards device miniaturization, there is considerable interest in multiferroic materials which exhibit both magnetic order and electrical polarization<sup>1-7</sup>. The hexagonal manganite  $RMnO_3$ <sup>8,9</sup> (where  $R$  is a rare-earth element with relatively small ionic radius) is a prototypical example of the so-called type-I multiferroics<sup>10</sup> with ferroelectric order at  $T_c \sim 900$  K<sup>11</sup> and an antiferromagnetic (AFM) order at much lower temperature,  $T_N \sim 100$  K<sup>12</sup>. A large dielectric anomaly occurs at  $T_N$ <sup>13-15</sup> indicating strong magnetoelectric (ME) coupling in these materials. There has been a large amount of experimental work in recent years, with the aim to understand the microscopic mechanism for the coupling between magnetic and electric degrees of freedom in these materials. Although it is generally believed that the spin-lattice coupling plays an important role in determining the complex properties in  $RMnO_3$ , much is unclear concerning the factors that influences the magnitude of the ME coupling<sup>16,17</sup>. In this Letter, we use inelastic neutron scattering (INS) and dielectric constant measurements to show that the magnitude of the ME coupling in multiferroic  $Y_{0.7}Lu_{0.3}MnO_3$  is directly coupled to the strength of the Mn trimerization distortion in these materials in the AFM phase. Our results thus provide direct evidence that the Mn trimerization is responsible for the ME effect and multiferroic phenomenon in  $Y_{1-y}Lu_yMnO_3$ .

The undoped compounds  $YMnO_3$  and  $LuMnO_3$  are characteristic hexagonal manganites where the  $Mn^{3+}$  ions (Mn  $x$  position at  $x \sim 1/3$ ) form a nearly ideal triangular lattice in the  $ab$ -plane above  $T_N$ .  $YMnO_3$  and  $LuMnO_3$  undergo AFM transitions (to two different magnetic structures) at  $T_N \sim 75$  K and  $T_N \sim 88$  K respectively, accompanied by an isostructural transition with large atomic displacement for all atoms in the unit cell. In particular, a distinct change of the Mn atomic po-

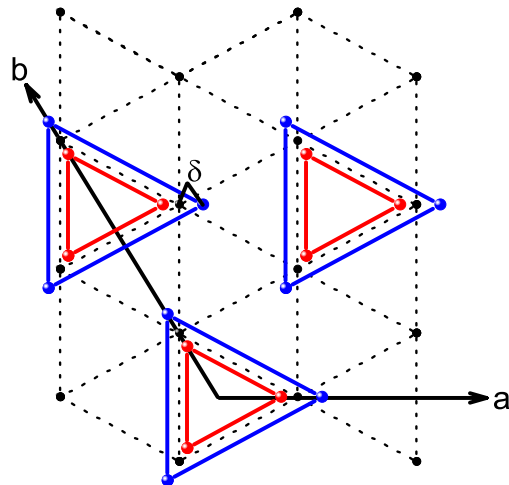


FIG. 1. (Color online) Schematic drawing of the Mn trimerization distortion below  $T_N$ . The dotted line depicts the ideal triangular lattice in the hexagonal  $ab$  plane with the Mn (filled black circle)  $x$  position at  $x_c = 1/3$ . The blue and red balls represent the Mn position  $x$  in the  $z = 0$  plane for  $YMnO_3$  and  $LuMnO_3$  illustrating opposite distortion directions of the Mn trimers, expansion in  $YMnO_3$  and contraction in  $LuMnO_3$ , respectively.  $\delta = |x - x_c|$  is the trimerization distortion parameter as described in the text.

sition, namely the Mn trimerization distortion, occurs in the basal plane at  $T_N$ <sup>17</sup>. As illustrated in Fig. 1, the Mn trimers distort in opposite directions in  $YMnO_3$  and  $LuMnO_3$ , expanding for  $YMnO_3$  and contracting for  $LuMnO_3$ . A recent theoretical study finds that the different magnetic structures of  $YMnO_3$  and  $LuMnO_3$  are determined by the different trimerization directions in these compounds<sup>18</sup>. Moreover, the dielectric anomaly at  $T_N$  is observed only in  $\epsilon_{ab}$  but not in  $\epsilon_c$  for both  $YMnO_3$

and  $\text{LuMnO}_3$ <sup>15</sup>. Although these studies suggest that the Mn trimerization may play a key role in determining the magnetic structure and the ME effects in  $\text{Y}_{1-y}\text{Lu}_y\text{MnO}_3$ , there are no experimental studies to determine the connection between the Mn trimerization and ME coupling.  $\text{Y}_{1-y}\text{Lu}_y\text{MnO}_3$  is an ideal system for such a study due to the following reasons: (1) since both Y and Lu are non-magnetic,  $\text{Y}_{1-y}\text{Lu}_y\text{MnO}_3$  is a clean system to study the magnetism of the Mn triangular lattice and its correlation with the ME effects; (2) the strength of the Mn trimerization distortion can be tuned in  $\text{Y}_{1-y}\text{Lu}_y\text{MnO}_3$ . With increasing Lu concentration, the Mn atomic position  $x$  changes from 0.340 for  $\text{YMnO}_3$ , larger than  $x_c=1/3$  for an ideal triangular lattice, to 0.331 for  $\text{LuMnO}_3$ , smaller than  $1/3$ . At  $y\sim 0.3$  Lu doping, the Mn atomic position  $x$  crosses the critical value  $x_c=1/3$  with a perfect triangular lattice without trimerization distortion<sup>19</sup>.

All measurements reported here were performed on single crystal samples. Large  $\text{Y}_{1-y}\text{Lu}_y\text{MnO}_3$  single crystals with nominal value of  $y=0.3$  were grown by the floating zone method under 4 atmospheres of oxygen flow. The crystals cut from the long rods were then annealed at 1350°C for 24 hours in a flowing argon atmosphere. For the magnetic susceptibility and dielectric constant measurements, the single crystal was cut into thin plates with  $ab$ -axes lying in the plane and  $c$ -axis pointing out of the plane. The magnetic susceptibility was measured using a Quantum Design Magnetic Properties Measurement System with magnetic field applied along the  $c$ -axis. The dielectric constant was measured using a LRC meter with electric field applied perpendicular and parallel to the  $c$ -axis and data were taken at 3.5 V ac driving voltage and 100 kHz frequency.

A single crystal with a mass of  $\sim 4$  gram was used for the neutron scattering experiments. The crystal was mounted on an aluminum plate and oriented in the  $(H\ 0\ L)$  scattering plane. The sample was then sealed in aluminum sample can under helium atmosphere and cooled using a closed-cycle He refrigerator. The neutron experiments were carried out using the HB-1A and CTAX triple-axis spectrometers (TAS) located at the High Flux Isotope Reactor (HFIR), and the Hybrid Spectrometer (HYSPEC) located at the Spallation Neutron Source (SNS) at Oak Ridge National Laboratory. HB-1A is a fixed incident energy TAS ( $E_i=14.64$  meV), and CTAX is a cold neutron TAS. Collimations of 48'-48'-sample-40'-80' downstream from the reactor to the detector was used for the HB-1A experiment with two pyrolytic graphite (PG) filters placed before the sample to eliminate higher-order contaminations in the beam. The CTAX experiment was performed with a fixed final energy of  $E_f=3$  meV (energy resolution is  $\sim 0.1$  meV FWHM at elastic condition) and collimations of guide-open-sample-80'-open. Higher-order contaminations were removed by a cooled Be filter placed between the sample and the analyzer. The HYSPEC experiment was carried out using an incident energy of  $E_i=25$  meV with a Fermi chopper spinning at 420 Hz.

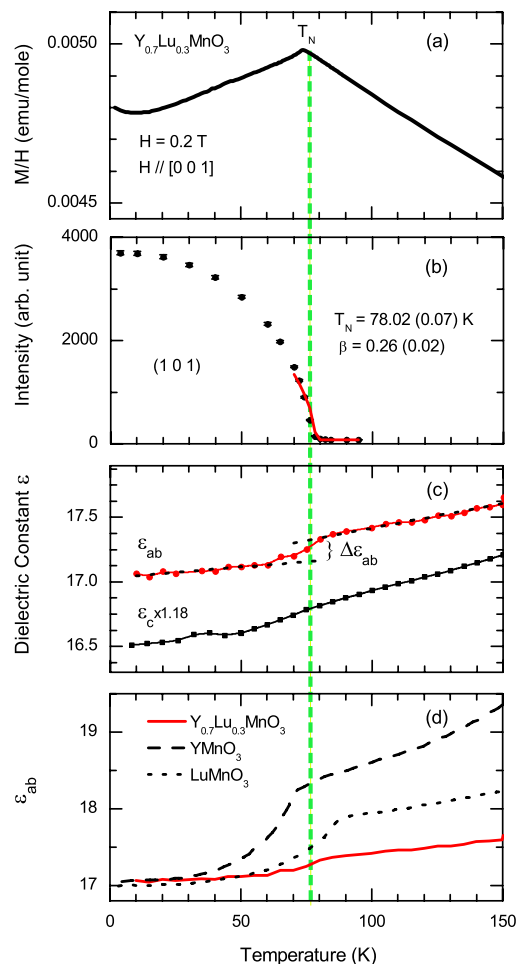


FIG. 2. (Color online) Magnetic susceptibility, magnetic order parameter and dielectric constant measurements of  $\text{Y}_{0.7}\text{Lu}_{0.3}\text{MnO}_3$ . The dashed green line depicts the Neel temperature  $T_N$ . (a) Magnetic susceptibility versus temperature measured with applied magnetic field parallel to the  $c$ -axis. (b) Integrated intensity of the  $(1\ 0\ 1)$  magnetic Bragg reflection as a function of temperature. The solid red line is a fit of the data to the power law as described in the text. (c) In-plane and out-of-plane dielectric constant measured with the electric field applied perpendicular and parallel to the  $c$ -axis.  $\Delta\epsilon_{ab}$  represents the critical in-plane dielectric constant change at  $T_N$ . (d) Comparison of the in-plane dielectric constant  $\epsilon_{ab}$  between  $\text{YMnO}_3$ ,  $\text{LuMnO}_3$  and  $\text{Y}_{0.7}\text{Lu}_{0.3}\text{MnO}_3$ . The data for  $\text{YMnO}_3$  ( $\epsilon_{ab}=2.1$ ) and  $\text{LuMnO}_3$  ( $\epsilon_{ab}=0.3$ ) are from Ref. 15 and are plotted with an offset of -2.1 and 0.3 for  $\text{YMnO}_3$  and  $\text{LuMnO}_3$ , respectively.

The  $\text{Y}_{0.7}\text{Lu}_{0.3}\text{MnO}_3$  sample was characterized by the magnetic susceptibility and neutron scattering magnetic order parameter measurements. Fig. 2 (a) shows the magnetic susceptibility measured with  $H \parallel c$  exhibiting a kink at  $\sim 78$  K indicating the AFM transition. The order parameter plotted in Fig. 2 (b) was measured by monitoring the strong magnetic Bragg peak  $(1\ 0\ 1)$  as a function of temperature. The integrated intensity was obtained by fitting the  $(1\ 0\ 1)$  rocking curve measured

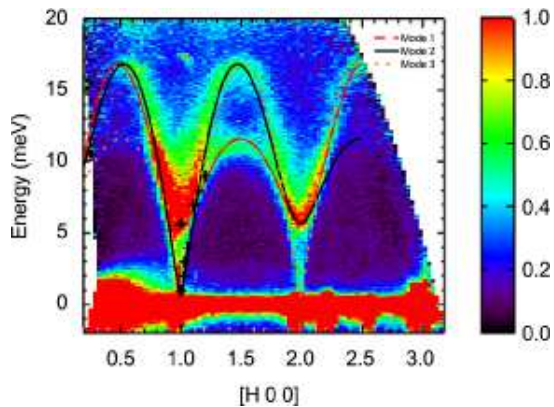


FIG. 3. (Color online) INS spectra of  $Y_{0.7}Lu_{0.3}MnO_3$  along  $(H\ 0\ 0)$  from the HYSPEC measurements at 4 K. The crossed symbols are data points obtained from TAS measurements. The lines are the calculated dispersion using the fitting parameters as described in the text.

at each temperature to a Gaussian function with a constant background. As illustrated by the dashed green line, the AFM transition at  $T_N \sim 78$  K was observed in both measurements consistent with previous reports<sup>19</sup>. The solid red line in Fig. 2 (b) is a fit to a power-law  $I(T) = I_0[(T_N - T)/T_N]^{2\beta}$  that yields  $T_N \approx 78.02 \pm 0.07$  K and  $\beta \approx 0.26 \pm 0.02$ , where  $\beta$  is the critical exponent. The yielded  $\beta$  value  $\sim 0.26$  is between the theoretical values of a 2D ( $\beta = 0.125$ ) and a 3D ( $\beta = 0.326$ ) Ising system in good agreement with a prior study<sup>20</sup>.

The spin dynamics of the  $Mn^{3+}$  ions has been investigated in detail in  $YMnO_3$ ,  $LuMnO_3$ , and  $HoMnO_3$ <sup>20–24</sup>. Fig. 3 shows the INS spectra of  $Y_{0.7}Lu_{0.3}MnO_3$  at 4K projected along the  $(H\ 0\ 0)$  direction. The measured spectra is very similar to that reported for  $YMnO_3$  and  $LuMnO_3$ . At  $(1\ 0\ 0)$ , two anisotropy gaps  $\Delta_1$  and  $\Delta_2$  were observed for both  $YMnO_3$  and  $LuMnO_3$ ,  $\Delta_1 \approx 2.4$  meV and  $\Delta_2 \approx 5.4$  meV for  $YMnO_3$ <sup>20</sup>, and  $\Delta_1 \approx 2.5$  meV and  $\Delta_2 \approx 6.5$  meV for  $LuMnO_3$ <sup>24</sup>, respectively. Compared to the parent compounds, our measurements show a much smaller  $\Delta_1$  gap in  $Y_{0.7}Lu_{0.3}MnO_3$ . The same sample was then measured using both cold and thermal TAS at HFIR to better characterize the two gaps in  $Y_{0.7}Lu_{0.3}MnO_3$ .

A summary of the TAS data along the  $c$ -axis is shown in Fig. 4. As illustrated in Fig. 4 (a),  $\Delta_1 \approx 0.52$  meV at  $(1\ 0\ 0)$  and the excitation shifts to  $\sim 1.5$  meV at  $(1\ 0\ 0.4)$ . On the other hand, the  $\Delta_2 \approx 5.56$  meV excitation shows no  $L$  dependence as depicted in Fig. 4 (b). Fig. 4 (c) plots the dispersion curves along the  $L$  direction for both excitations constructed from a series of energy scans at constant wave-vector. The data points were determined by fitting the energy scans at constant wave-vector assuming Gaussian peak-shapes. The 0.52 meV gap shows modest dispersion along the  $L$ -direction with a maximum energy shift of  $\sim 1.5$  meV and the 5.56 meV gap is dispersionless along  $L$  within the instrumental resolution. The TAS data points along  $H$  are plotted in Fig. 3 to

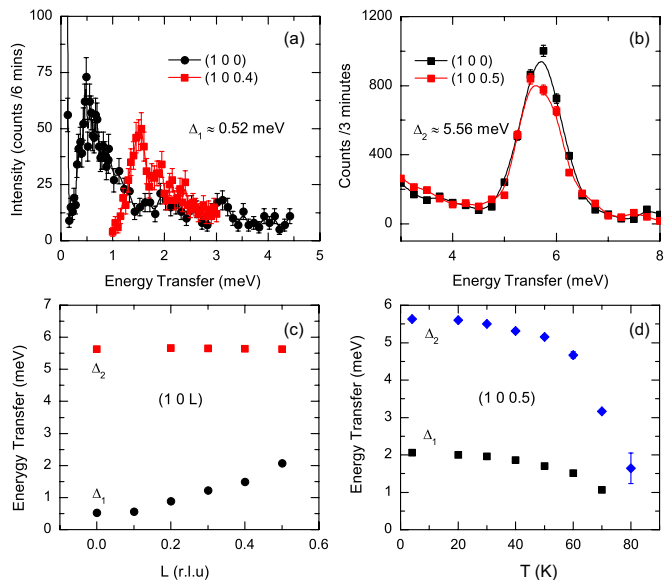


FIG. 4. (Color online) Magnetic excitations in  $Y_{0.7}Lu_{0.3}MnO_3$  measured using triple-axis spectrometers. (a) The  $\Delta_1 \approx 0.52$  meV gap and its  $q$ -dependence along  $L$  comparing constant wave-vector scans measured at  $(1\ 0\ 0)$  and  $(1\ 0\ 0.4)$  using the CG-4C cold neutron TAS at  $T = 4$  K. (b) The  $\Delta_2 \approx 5.56$  meV gap and its  $q$ -dependence along  $L$  comparing constant wave-vector scans measured at  $(1\ 0\ 0)$  and  $(1\ 0\ 0.5)$  at  $T = 4$  K using the HB-1A thermal neutron TAS. (c) Spin wave dispersion along the  $L$ -direction measured at 4 K. (d) Temperature evolution of the magnetic excitations measured at  $(1\ 0\ 0.5)$ .

show a good agreement with the HYSPEC data. Weak dispersions were observed along  $L$  out of the hexagonal plane and strong dispersions were observed along  $H$  in the hexagonal plane consistent with the layered magnetic structure of  $Y_{1-y}Lu_yMnO_3$ . Fig. 4 (d) shows the temperature evolution of the excitations measured at  $(1\ 0\ 0.5)$ . The energy of both excitations decrease with increasing temperature and vanish at  $T_N$  confirming their magnetic origin. In summary, the  $q$  and temperature dependence of the magnetic spectra of  $Y_{0.7}Lu_{0.3}MnO_3$  show very similar behavior comparing to  $YMnO_3$  and  $LuMnO_3$  except for the significantly smaller  $\Delta_1 \approx 0.52$  meV.

In order to make a quantitative comparison between  $YMnO_3$ ,  $Y_{0.7}Lu_{0.3}MnO_3$ , and  $LuMnO_3$ , we model the dispersion of the magnetic excitations in Fig. 3 using the same linear spin wave analysis that has been applied to analyze the  $HoMnO_3$  and  $YMnO_3$  INS data<sup>20,21</sup>. The model, defined by the Hamiltonian  $\mathcal{H} = J \sum_{\langle i,j \rangle} \mathbf{S}_i \cdot \mathbf{S}_j + D_y \sum_i (\mathbf{S}_i^y)^2 + D_z \sum_i (\mathbf{S}_i^z)^2$ , takes into account the nearest-neighbor exchange interaction  $J$ , and two single ion anisotropy terms  $D_y$  and  $D_z$  representing the in-plane and out-of-plane anisotropy constants, respectively. Three modes are obtained with the following dispersion

TABLE I. Compare the lattice constants (space group  $P6_3cm$ ),  $T_N$ , trimerization distortion parameter  $\delta$ , exchange constant  $J$ , single ion anisotropy parameters  $D_y$ ,  $D_z$ , and the critical dielectric constant change  $\Delta\varepsilon_{ab}$  between  $\text{YMnO}_3$ ,  $\text{LuMnO}_3$  and  $\text{Y}_{0.7}\text{Lu}_{0.3}\text{MnO}_3$ .

	Lattice ( $\text{\AA}$ )	$T_N$ (K)	$\delta$	$J$ (meV)	$D_y$ (meV)	$D_z$ (meV)	$\Delta\varepsilon_{ab}$	Refs.
$\text{YMnO}_3$	$a=6.132, c=11.452$	75	0.007	2.4	0.033	0.32	1.02	Ref.20
$\text{Y}_{0.7}\text{Lu}_{0.3}\text{MnO}_3$	$a=6.103(2), c=11.403(1)$	78	0.001	2.57(5)	0.0017(2)	0.35(1)	0.17	This Work
$\text{LuMnO}_3$	$a=6.05, c=11.4$	88	0.003	2.9	0.035	0.4	0.77	Ref.24

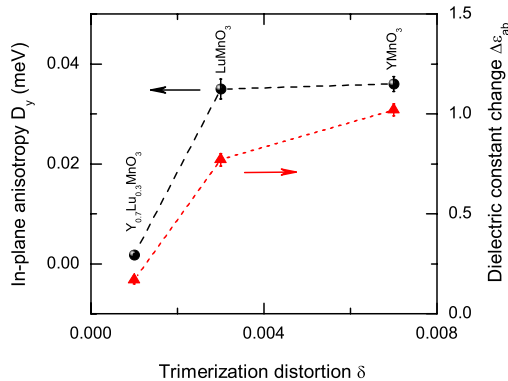


FIG. 5. (Color online) In-plane single ion anisotropy  $D_y$  versus trimerization distortion  $\delta$  (ball, left axis), and critical dielectric constant change  $\Delta\varepsilon_{ab}$  versus  $\delta$  (triangle, right axis) for  $\text{Y}_{0.7}\text{Lu}_{0.3}\text{MnO}_3$ ,  $\text{YMnO}_3$ , and  $\text{LuMnO}_3$ .

equation:

$$\hbar\omega_i = 3JS\sqrt{[(1 + 4z_i + 2D_z/3J)(1 - 2z_i + 2D_y/3J)]}, \quad (1)$$

where  $z_i$  ( $i = 1, 2$  or  $3$ ) is defined by lattice Fourier sums identical to Ref. 21, and  $S = 2$  for  $\text{Mn}^{3+}$  ions. A fit to the data using Eq. 1 yields  $J = 2.57$  (0.05) meV,  $D_y = 0.0017$  (0.0002) meV, and  $D_z = 0.35$  (0.01) meV. Our INS data can be well described by the model as depicted in Fig. 3 comparing the three spin wave modes calculated using the fitting parameters to the measured magnetic spectra. The obtained fitting parameters are listed in Table I in comparison with the results for  $\text{YMnO}_3$  and  $\text{LuMnO}_3$ <sup>25</sup>. The lattice constants,  $T_N$ ,  $J$  and  $D_z$  values of  $\text{Y}_{0.7}\text{Lu}_{0.3}\text{MnO}_3$  all fall in between the values of  $\text{YMnO}_3$  and  $\text{LuMnO}_3$ . This is consistent with the lattice parameters and unit cell volume being contracted from  $\text{YMnO}_3$  to  $\text{LuMnO}_3$ . However, a much smaller  $D_y$  value was obtained for  $\text{Y}_{0.7}\text{Lu}_{0.3}\text{MnO}_3$ .

At the zone center, the energy of the two magnetic excitations can be described as  $\Delta_1 = 3JS[(2D_y/3J)(3)]^{1/2}$  and  $\Delta_2 = 3JS[(2D_z/3J)(3/2)]^{1/2}$  corresponding to the in-plane and out-of-plane single ion anisotropy gaps<sup>20</sup>. Unlike  $\text{YMnO}_3$  and  $\text{LuMnO}_3$  which have almost the same value of  $\Delta_1 \sim 2.5$  meV regardless the opposite trimerization distortion direction in these materials, a smaller in-plane anisotropy gap  $\Delta_1 \sim 0.52$  meV was observed in  $\text{Y}_{0.7}\text{Lu}_{0.3}\text{MnO}_3$  that yields a significantly smaller  $D_y \sim$

0.0017 meV value. Previous systematic study indicates that the Mn atomic position in  $\text{Y}_{0.7}\text{Lu}_{0.3}\text{MnO}_3$  is very close to the critical value ( $x \sim 1/3$ )<sup>19</sup>, the Mn trimerization distortion in  $\text{Y}_{0.7}\text{Lu}_{0.3}\text{MnO}_3$  is much weaker comparing to  $\text{YMnO}_3$  and  $\text{LuMnO}_3$ . The in-plane single ion anisotropy  $D_y$  is coupled to the Mn trimerization in the hexagonal plane thus is very sensitive to the strength of trimerization distortion<sup>18</sup>. We attribute the observed small in-plane anisotropy gap to the weaker Mn trimerization distortion in  $\text{Y}_{0.7}\text{Lu}_{0.3}\text{MnO}_3$ . It is thus of great interest to see how the weaker Mn trimerization distortion affects the magnitude of the ME coupling. If the ME effect is directly linked to the Mn trimerization distortion, we would expect a much weaker in-plane dielectric anomaly in  $\text{Y}_{0.7}\text{Lu}_{0.3}\text{MnO}_3$  which is indeed what we observed in the dielectric constant measurements. As illustrated in Fig. 2 (c), at  $T_N$ , no anomaly was observed in  $\varepsilon_c$  consistent with previous reports, whereas a weaker dielectric anomaly was observed in  $\varepsilon_{ab}$ . Fig. 2 (d) compares the in-plane dielectric constant  $\varepsilon_{ab}$  between  $\text{YMnO}_3$ ,  $\text{LuMnO}_3$  and  $\text{Y}_{0.7}\text{Lu}_{0.3}\text{MnO}_3$  ( $\varepsilon_{ab}$  values for  $\text{YMnO}_3$  and  $\text{LuMnO}_3$  are taken from Ref. 15 and plotted in Fig. 2 (d) with a -2.1 and 0.3 offset, respectively) and it clearly shows that the dielectric anomaly observed in  $\text{Y}_{0.7}\text{Lu}_{0.3}\text{MnO}_3$  is much weaker comparing to  $\text{YMnO}_3$  and  $\text{LuMnO}_3$ .

Table I compares our  $\text{Y}_{0.7}\text{Lu}_{0.3}\text{MnO}_3$  results to the ones reported for  $\text{YMnO}_3$  and  $\text{LuMnO}_3$  from the previous study. We define a trimerization distortion parameter  $\delta$  to reflect the strength of the trimerization distortion,  $\delta = |x - x_c|$  as depicted in Fig. 1. The  $\delta$  values listed in Table I are based on the data reported in Ref. 19. We also define a critical dielectric constant change parameter  $\Delta\varepsilon_{ab}$  to represent the magnitude of the ME coupling at  $T_N$ . As shown in Fig. 2 (c), the  $T < T_N$  and  $T > T_N$   $\varepsilon_{ab}$  data are fit to a linear function respectively, and  $\Delta\varepsilon_{ab}$  is the difference between these two fittings at  $T_N$ . The  $D_y$  vs.  $\delta$  and  $\Delta\varepsilon_{ab}$  vs.  $\delta$  for  $\text{YMnO}_3$ ,  $\text{Y}_{0.7}\text{Lu}_{0.3}\text{MnO}_3$ , and  $\text{LuMnO}_3$  are plotted in Fig. 5. It shows that both  $D_y$  and  $\Delta\varepsilon_{ab}$  decrease with decreasing  $\delta$  indicating strong correlations between the strength of trimerization distortion and the magnitude of ME coupling.

In summary, our INS study of  $\text{Y}_{0.7}\text{Lu}_{0.3}\text{MnO}_3$  reveals a small in-plane single ion anisotropy gap that coincides with a weaker dielectric anomaly in  $\varepsilon_{ab}$ . This is attributed to a much weaker Mn trimerization distortion in  $\text{Y}_{0.7}\text{Lu}_{0.3}\text{MnO}_3$  due to the doping influence of the Mn atomic position  $x \sim 1/3$ . These results provide

strong evidence that the Mn trimerization is responsible for the ME effect in  $Y_{1-y}Lu_yMnO_3$  and the magnitude of ME coupling is coupled to the strength of the trimerization distortion. High resolution neutron diffraction study have shown that the Mn trimerization is a systematic feature in  $RMnO_3$ <sup>26</sup>, this finding may shed light on a deeper understanding of the multiferroic phenomenon in this series of materials inviting further theoretical investigations.

We acknowledge valuable discussions with Randy Fishman. Work at the High Flux Isotope Reactor and Spallation Neutron Source, Oak Ridge National Laboratory, was sponsored by the Scientific User Facilities Division, Office of Basic Energy Sciences, U.S. Department of Energy. The single crystal growth and neutron scattering work at UTK/Rice is supported by the U.S. DOE BES under Grant No. DE-FG02-05ER46202.

- 
- \* wt6@ornl.gov  
† tanbj2008@gmail.com
- <sup>1</sup> M. Fiebig, *J. Phys. D: Appl. Phys.* **38**, R123 (2005).
  - <sup>2</sup> N. A. Spaldin and M. Fiebig, *Science* **309**, 391 (2005).
  - <sup>3</sup> Y. Tokura, *Science* **312**, 1481 (2006).
  - <sup>4</sup> W. Eerenstein, N. D. Mathur, and J. F. Scott, *Nature* **442**, 759 (2006).
  - <sup>5</sup> T. Kimura, T. Goto, H. Shintani, K. Ishizaka, T. Arima, and Y. Tokura, *Nature* **426**, 55 (2003).
  - <sup>6</sup> N. Hur, S. Park, P. A. Sharma, J. S. Ahn, S. Guha, and S. W. Cheong, *Nature* **429**, 392 (2004).
  - <sup>7</sup> S.-W. Cheong and M. Mostovoy, *Nat. Mater.* **6**, 13 (2007).
  - <sup>8</sup> M. Fiebig, Th. Lottermoser, D. Fröhlich, A. V. Goltsev, and R. V. Pisarev, *Nature* **419**, 818 (2002).
  - <sup>9</sup> T. Lottermoser, T. Lonkai, U. Amann, D. Hohlwein, J. Ihringer, and M. Fiebig, *Nature* **430**, 541 (2004).
  - <sup>10</sup> A.B. Harris, and G. Lawes, *Ferroelectricity in incommensurate magnets*, in *The handbook of Magnetism and Advanced Magnetic Materials*, Wiley, London, 2006. (e-print cond-mat/0508617)
  - <sup>11</sup> T. Choi, Y. Horibe, H. T. Yi, Y. J. Choi, W. Wu, and S.-W. Cheong, *Nat. Mater.* **9**, 253 (2010).
  - <sup>12</sup> D. G. Tomuta, S. Ramakrishnan, G. J. Nieuwenhuys, and J. A. Mydosh, *J. Phys.: Condens. Matter* **13**, 4543-4552 (2001).
  - <sup>13</sup> Nobuyuki Iwata and Kay Kohn, *J. Phys. Soc. Jpn.* **67**, 3318-3319 (1998).
  - <sup>14</sup> Z. J. Huang, Y. Cao, Y. Y. Sun, Y. Y. Xue, and C. W. Chu, *Phys. Rev. B* **56**, 2623 (1997).
  - <sup>15</sup> T. Katsufuji, S. Mori, M. Masaki, Y. Moritomo, N. Yamamoto, and H. Takagi, *Phys. Rev. B* **64**, 104419 (2001).
  - <sup>16</sup> Bas B. Van Aken, and Thomas T. M. Palstra, *Phys. Rev. B* **69**, 134113 (2004).
  - <sup>17</sup> S. Lee, A. Pirogov, M. Kang, K.-H. Jang, M. Yonemura, T. Kamiyama, S.-W. Cheong, F. Gozzo, N. Shin, H. Kimura, Y. Noda, and J.-G. Park, *Nature (London)* **451**, 805 (2008).
  - <sup>18</sup> I. V. Solovyev, M. V. Valentyuk, and V. V. Mazurenko, *Phys. Rev. B* **86**, 054407 (2012).
  - <sup>19</sup> J. Park, S. Lee, M. Kang, K.-H. Jang, C. Lee, S. V. Streltsov, V. V. Mazurenko, M. V. Valentyuk, J. E. Medvedeva, T. Kamiyama, and J.-G. Park, *Phys. Rev. B* **82**, 054428 (2010).
  - <sup>20</sup> Tapan Chatterji, S. Ghosh, A. Singh, L. P. Regnault, and M. Rheinstädter, *Phys. Rev. B* **76**, 144406 (2007).
  - <sup>21</sup> O. P. Vajk, M. Kenzelmann, J.W. Lynn, S. B. Kim, and S.-W. Cheong, *Phys. Rev. Lett* **94**, 087601 (2005).
  - <sup>22</sup> Junghwan Park, J.-G. Park, Gun Sang Jeon, Han-Yong Choi, Changhee Lee, W. Jo, R. Bewley, K. A. McEwen, and T. G. Perring, *Phys. Rev. B* **68**, 104426 (2003).
  - <sup>23</sup> T. J. Sato, S. -H. Lee, T. Katsufuji, M. Masaki, S. Park, J. R. D. Copley, and H. Takagi, *Phys. Rev. B* **68**, 014432 (2003).
  - <sup>24</sup> H. J. Lewtas, A. T. Boothroyd, M. Rotter, D. Prabhakaran, H. Müller, M. D. Le, B. Roessli, J. Gavilano, and P. Bourges, *Phys. Rev. B* **82**, 184420 (2010).
  - <sup>25</sup> The listed  $J$ ,  $D_y$ , and  $D_z$  values for  $LuMnO_3$  in Table I were obtained by refitting the data in Ref. 24 using the same model.
  - <sup>26</sup> X. Fabrèges, S. Petit, I. Mirebeau, S. Pailhès, L. Pinsard, A. Forget, M. T. Fernandez-Diaz, and F. Porcher, *Phys. Rev. Lett* **103**, 067204 (2009).